植物学报 *Chinese Bulletin of Botany* 2025, **60** (4): 515–532, www.chinbullbotany.com
doi: 10.11983/CBB24112 cstr: 32102.14.CBB24112

·研究论文·

一个新的黄瓜叶色突变体鉴定、初定位及转录组分析

赵蔓雅, 孙倩楠, 徐晶晶, 段恬妮, 蔡锦涛, 周婧, 范婷婷, 萧浪涛*, 王若仲*

湖南农业大学生物科学技术学院, 植物激素与生长发育湖南省重点实验室, 长沙 410128

摘要 叶色突变体是研究光形态发生、叶绿体发育、叶绿素代谢和光合作用机制等多种生理过程的理想材料。该研究从黄瓜(*Cucumis sativus*) XYYH-2-1-1株系自交后代中获得1个新的黄化致死突变体*ycl* (*yellow cotyledon lethal*)。该突变体自幼苗出土后子叶一直呈黄化状态, 约2周后枯萎死亡, 其生长抑制表型为非光依赖型。与野生型相比, *ycl*突变体的Chl *a*和Chl *b*含量趋于零, 叶绿素生物合成途径中Mg^{2+}螯合过程受阻。显微和超微结构分析发现, *ycl*叶片组织紊乱、叶绿体发育受阻。*ycl*的抗氧化酶活性及丙二醛含量显著升高, 说明其受到氧化胁迫, 且抗氧化能力强。*ycl*净光合速率极显著降低, 胞间CO_2浓度上升, 推测*ycl*光合速率降低源于气孔导度降低、叶绿素含量减少和叶绿体发育受阻。转录组学分析表明, *ycl*与其野生型间存在337个差异表达基因, 光合作用、类黄酮生物合成、叶绿素代谢和活性氧代谢是导致*ycl*黄化致死表型形成的关键途径。通过BSA-Seq分析, *ycl*突变基因初步定位于3号染色体的1.48–1.9 Mb区间, 内含41个候选基因。对*ycl*突变体的研究为阐明黄瓜叶绿体发育的分子机制提供了参考。

关键词 黄瓜, 黄化致死突变体*ycl*, 生理特性, 基因定位, 转录组分析

赵蔓雅, 孙倩楠, 徐晶晶, 段恬妮, 蔡锦涛, 周婧, 范婷婷, 萧浪涛, 王若仲 (2025). 一个新的黄瓜叶色突变体鉴定、初定位及转录组分析. 植物学报 **60**, 515–532.

黄瓜(*Cucumis sativus*)是主要的蔬菜作物之一。光合作用与黄瓜的果实产量密不可分, 叶色在很大程度上决定了光合效率。因此, 叶色突变体是研究光形态发生、叶绿体发育和光合作用机制等多种生理过程的理想材料(Stern et al., 2004; Zhu et al., 2016; Gao et al., 2016)。

叶色突变体在玉米(*Zea mays*) (Zhong et al., 2015; Guan et al., 2016)、甜瓜(*C. melo*) (Liu et al., 2019; Han et al., 2023)以及西瓜(*Citrullus lanatus*) (Zhu et al., 2019; Xu et al., 2023)等作物中均有报道, 如使用CRISPR/Cas9技术获得的水稻(*Oryza sativa*)白化叶色突变体*osppr16d*和*osppr16s* (Huang et al., 2020)以及叶色随温度变化的水稻温敏感叶色突变体*Jiahua No.1* (陈佳颖等, 2010)和叶绿素缺乏的黄色大豆(*Glycine max*)突变体*MinnGold* (Sakowska et al., 2018)。随着分子生物学和基因组学的进一步发展, 我国对叶色突变体的研究日渐深入, 参与叶绿素代谢途径的基因突变是目前报道较多的一类, 如5-氨基乙酰丙酸(5-aminolevulinic acid, 5-ALA) (Ladygin, 2006; Deng et al., 2017)和Mg-原卟啉IX (Mg-protoporphyrin IX, Mg-Proto IX) (Zhao et al., 2020a; Shim et al., 2023)的合成。Nagata等(2005)通过甲基磺酸乙酯(ethyl methane sulfonate, EMS)诱变在拟南芥(*Arabidopsis thaliana*)中分离出1个浅绿色突变体*dvr,* 其在弱光环境下能正常光合作用, 但在强光下迅速死亡, 叶绿素*a*/*b*比值增大, 通过图位克隆发现是由叶绿素生物合成中最后一步*DVR*基因发生了碱基突变引起。Gao等(2016)发现黄瓜叶色突变体*C528*产生黄叶是由于编码镁螯合酶I亚基的基因*CsChlI*发生了单核苷酸突变。Song等(2018)鉴定了一种表现出色素含量降低和叶绿体发育延迟的黄瓜黄绿叶突变体, 该突变体的产生是由于参与质体发育的DnaJ-类锌指蛋白编码基因发生了单核苷酸突变。黄瓜作为葫芦科模式植物, 已报道了23种叶色突变体,

收稿日期: 2024-07-23; 接受日期: 2025-06-04
基金项目: 湖南省教育厅科技计划(No.20B306)
* 通讯作者。E-mail: ltxiao@hunau.edu.cn; wangruozhong@hunau.edu.cn

其中8个叶色突变体完成了染色体定位及克隆(Pierce and Wehner, 1990; Gao et al., 2016; Miao et al., 2016; Song et al., 2018; Ding et al., 2019; Zhang et al., 2020b, 2022; Hu et al., 2020; Xiong et al., 2021)。迄今, 在各类黄瓜叶色突变体中, 叶绿体发育缺陷、光合作用受阻的致死型突变体有6个, 即*al*、*cd*、*gc*、*ls*、*pl*以及*yl2.1* (Pierce and Wehner, 1990; Xiong et al., 2021)。其中, Xiong等(2021)报道了一种黄叶突变体*yl2.1*, 他们通过定位将编码磷酸丙糖异构酶(triose phosphate isomerase, TPI)质体亚型的*Cs-YL2.1*作为候选基因, 该基因突变会影响叶绿体的发育, *yl2.1*出现幼苗致死。在水稻中, 发现突变体*vsl1*在播种2周后叶尖出现红棕色斑点, 随着植株的发育, 叶尖上的病斑逐渐扩散至叶基部, 直至覆盖整个叶片, 属于致死型叶色突变(Yin et al., 2015)。这些突变体为研究光形态发生(Parks and Quail, 1991)、叶绿体发育(Wu et al., 2007; Mao et al., 2019)、叶绿素生物合成(Qin et al., 2017)和光合作用机制(Zhong et al., 2015; Huang et al., 2016; Sakowska et al., 2018)提供了理想的遗传材料, 但有关黄化致死表型的分子机制尚不十分清楚。

本研究前期从黄瓜XYYH-2-1-1株系中分离获得1个能稳定遗传的黄化致死突变体*ycl*, 从表型特征和遗传区域来看, 该突变体是一个新的黄瓜叶色突变体。通过对*ycl*进行表型鉴定、叶片显微结构及叶绿体结构观察、生理生化指标测定、转录组分析及突变基因初步定位, 为解析*ycl*黄化致死表型产生的分子机制奠定了基础。

1 材料与方法

1.1 黄瓜材料及表型鉴定

黄瓜(*Cucumis sativus* L.)黄化致死突变体*ycl*是通过黄瓜XYYH-2-1-1株系自交性状分离获得, 为自然突变体, 其突变性状稳定遗传。由于突变体在子叶期黄化致死, 突变基因仅能通过杂合体保存, 因此将杂合株系自交产生的后代播种后, 即可分离获得黄化苗, 黄化苗株系可确定为杂合株; XYYH-2-1-1后代中稳定遗传的正常绿叶表型XYYH-3-1则为野生型对照。播种野生型和杂合株系共92株, 构建野生型基因池、杂合体基因池和突变体基因池, 单株取样, 用于突变基因初步定位。以上材料均种植于湖南农业大学实验温室和植物激素与生长发育湖南省重点实验室植物培养室。亲本XYYH-2-1-1由湖南省蔬菜研究所陈惠明研究员惠赠, 于子叶期(播种后7天)对XYYH-3-1及*ycl*株系的株高、茎粗及叶面积进行评价, 重复3次, 每次重复测量5株。

挑选籽粒饱满的杂合体种子, 于50°C热水中浸泡30分钟, 用镊子剥去种皮。将种仁放入盛有无菌水的三角瓶中防止失水。先后通过75%乙醇消毒、无菌水清洗、0.3% NaClO溶液消毒和无菌水清洗, 期间轻轻摇晃三角瓶, 使其充分消毒与洗净。用滤纸吸除种子表层水分, 随后播种于含MS培养基的培养瓶中, 25°C黑暗条件下培养7天后拍照观察, 然后置于25°C光照条件下培养1天, 再次观察表型变化并拍照记录。

1.2 光合色素含量测定

采用紫外分光光度法测定光合色素含量。选取XYYH-3-1以及*ycl*子叶期样本的新鲜叶片, 经液氮处理并研磨后, 称取0.1 g, 置于95%乙醇中黑暗浸提, 离心后取上清液, 重复此步骤直至组织变白。随后, 使用Tecan-SPARK多功能酶标仪测定665、649及470 nm波长下的叶绿素*a*、叶绿素*b*和类胡萝卜素的吸光度。计算公式如下:

$$C\ (\text{Chl } a)=(13.95\times A_{665}-6.88\times A_{649})\times V/(1\ 000\times m)$$

$$C\ (\text{Chl } b)=(24.96\times A_{649}-7.32\times A_{665})\times V/(1\ 000\times m)$$

$$C\ (\text{Total Chl})=C\ (\text{Chl } a)+C\ (\text{Chl } b)$$

$$C\ (\text{Caro})=(1\ 000\times A_{470}-2.05C_a-114.8\times C_b)/245$$

其中, V为提取液的总体积(L); m为样品鲜重(g)。

1.3 叶绿素合成中间代谢产物含量测定

5-氨基乙酰丙酸(5-ALA)含量的测定参考Dei (1985)的方法, 用等体积的4%三氯乙酸缓冲液以及Ehrlich-Hg显色液作对比, 使用酶标仪测量553 nm处的OD值, 通过摩尔消光系数7.2×10^4 mol·cm^{-1}求出5-ALA含量。胆色素原(porphobilinogen, PBG)含量的测定参照Bogorad (1962)的方法, 利用酶标仪测得553 nm处的OD值, 通过摩尔消光系数6.1×10^4 mol·cm^{-1}求出PBG含量。尿卟啉原III (Uroporphyrinogen III, Urogen III)以及粪卟啉原III (coproporphyrinogen III, Coprogen III)含量测定参考Bogorad (1962)的方法, 测量萃取后的下层溶液在405.5 nm处的OD值, 采用摩

尔消光系数5.48×10^5 mol·cm^{-1}得出Urogen III的含量; 随后, 进一步萃取并测定盐酸相混合液在399.5 nm处的OD值, 通过系数4.89×10^5 mol·cm^{-1}即可计算Coprogen III的含量。原卟啉IX (protoporphyrin IX, Proto IX)和Mg-原卟啉IX含量测定参照Liu等(2015)的方法。分别测定上清液在575、590和628 nm处的OD值, 各叶绿素前体物质的含量以μg·g^{-1} FW表示。计算公式如下:

$C_{ProtoIX}=0.18016A_{575}-0.04036A_{628}-0.04515A_{590}$

$C_{Mg\text{-}ProtoIX}=0.06077A_{590}-0.01937A_{575}-0.003423A_{628}$

1.4 光合作用参数测定

使用Li-6400便携式光合测定仪, 测定XYYH-3-1与*ycl*子叶期叶片的胞间CO_2浓度(C_i)、气孔导度(G_s)、净光合速率(P_n)和蒸腾速率(T_r)。测试时间为温室培养的上午9:00–12:00。选用红蓝光源, 开放气路, 光照强度设定为1 000 μmol·m^{-2}·s^{-1}。重复3次, 每次测量5株。

1.5 叶片组织石蜡切片观察

选取播种7天的XYYH-3-1和*ycl*子叶期叶片, 用手术刀截取包含主叶脉在内的叶片中心部位, 面积约为3 cm × 3 cm, 立即放入装有FAA固定液的离心管固定, 依次使用不同浓度的乙醇梯度脱水, 二甲苯逐级透明, 石蜡浸蜡及包埋, 最后对包埋材料进行修整、脱蜡及染色。使用显微镜观察分析染色切片。

1.6 叶片透射电镜观察

选取播种7天且长势良好的XYYH-3-1和*ycl*叶片, 用手术刀截取4 mm × 4 mm叶片组织, 立即放入装有FAA固定液的棕色玻璃瓶固定, 依次使用不同浓度的乙醇逐级脱水, 丙酮配比812包埋剂包埋, 切片后用2%醋酸铀饱和乙醇溶液染色, 透射电子显微镜下观察, 采集图像进行分析。

1.7 抗氧化酶活性和丙二醛浓度测定

取XYYH-3-1和*ycl*子叶期叶片, 测定超氧化物歧化酶(superoxide dismutase, SOD)和过氧化物酶(peroxidase, POD)活性及丙二醛(malondialdehyde, MDA)含量。重复3次, 每次测量5株。酶液制备: 叶片加液氮研磨, 称取0.15 g样品于2 mL离心管, 加入1.5 mL 0.05 mol·L^{-1} (pH7.8)磷酸缓冲液, 旋涡混匀, 4°C下12 000 ×*g*冷冻离心15分钟, 取上清于4°C保存备用。SOD和POD活性测定分别采用氮蓝四唑法(李小方和张志良, 2016)和愈创木酚法(李小方和张志良, 2016), MDA浓度测定采用硫代巴比妥酸法(刘萍和李明军, 2016)。

1.8 BSA-Seq分析

采用混合分组分析(bulked segregation analysis, BSA) (Michelmore et al., 1991)对突变基因进行初定位。采用CTAB法提取基因组DNA并检测质量, 对第18号分离群体进行单基因BSA分析, 取子叶构建2个DNA池: 15棵绿色植株子叶构成18GP基因池、15棵黄化植株子叶构成18YP基因池。对18个群体的所有单株开展BSA-Seq分析, 取子叶构建3个DNA池: 10棵野生型植株子叶构成XYY-WT基因池、8个株系共25棵黄化植株子叶构成XYYpool基因池、8个株系共25棵杂合株系绿色植株子叶构成XYGpool基因池; 因取子叶构建的混池测序获得的差异SNP较少, 而当*ycl*及其野生型进入真叶期后, 光合作用等相关代谢基因表达水平差异更明显, 故取真叶构建了3个基因池: 10棵野生型植株真叶构成XYY-WTZ基因池、8个株系共25棵黄化植株真叶构成HHZSZ基因池、8个株系共25棵杂合株系绿色植株真叶构成XYGZ基因池。待检验合格后委托湖南拓唯生物科技有限公司进行全基因组重测序, 先使用Qubit2.0软件进行初定量, 随后将文库稀释至1 ng·μL^{-1}并对其insert size进行检测, 用Q-PCR法准确定量文库的有效浓度后使用illumina Novaseq6000仪测序, 得到全基因组测序结果。使用BWA软件将reads比对到黄瓜参考基因组, 使用SAMtools软件寻找全基因组的SNP位点, 最终确定目标基因所在的染色体和大致位置。

1.9 植物RNA的提取与qRT-PCR

收集长势良好的XYYH-3-1以及*ycl*子叶期根、茎、叶, 取样时用ddH_2O冲洗根部土壤, 滤纸吸干后立即放入液氮中速冻保存。采用美基生物HiPure Plant RNA Mini Kit (多糖多酚)提取RNA。用莫纳生物MonScript™ RTIII All-in-One Mix with dsDNase试剂盒进行反转录。引物设计参考葫芦科作物基因组数据库网站(http://cucurbitgenomics.org/)上介绍的方法, 并使用

NCBI的Primer BLAST工具(https://blast.ncbi.nlm.nih.gov/Blast.cgi)确定引物的质量与特异性，委托生工生物工程股份有限公司合成(表1)。cDNA合成后，以*Cs-Actin*为内参基因，对反转录合成的cDNA进行RT-PCR检测，合格后使用诺唯赞ChamQ Universal SYBR qPCR Master Mix进行实时荧光定量PCR (qRT-PCR)。将反转录得到的cDNA，根据半定量RT-PCR结果稀释2–10倍作为模板，以减少cDNA浓度过高造成的误差。以*Cs-Actin*为内参基因，根据Threshold cycle (Cq/Ct)值，采用$2^{-\Delta\Delta CT}$法计算基因的相对表达量(Schmittgen and Livak, 2008)。

1.10 转录组测序(RNA-Seq)分析

选取播种后40小时且长势良好的XYYH-3-1和*ycl*植株为RNA-Seq样本，并立即保存在液氮中。设3次生物学重复，每个重复随机取3株。提取总RNA并用NanoDrop 2000分光光度计对RNA浓度进行初定量，用Agilent 2100/4200对浓度进行精确定量。RNA样本检测合格后，依次通过mRNA富集、片段破碎、cDNA第1和第2链合成、碱基修复、polyA加尾、加测序接头、纯化和PCR扩增等环节构建文库。随后，使用illumina Novaseq6000仪对qPCR定量文库进行PE150测序。对测序原始数据进行质量评估以获得高质量的Clean reads。使用Bowtie2软件将Clean reads比对到silva数据库去除rRNA，剩下的Reads用于后续分析。采用Hisat2软件将去除rRNA后的Reads与黄瓜基因组ChiniseLong_V3进行比对，根据基因组注释文件指定的基因位置信息统计测序数据、参考基因组的比对率以及测序数据与参考基因组比对的区域分布。使用edgeR软件进行差异显著性分析，判定标准为$|\log_2(\text{Fold Change})|>1$且$q$-value<0.05。

1.11 数据统计分析

采用Microsoft Office Excel 2019软件进行数据统计，采用SPSS 24.0软件进行方差分析和差异显著性检验，用GraphPad Prism 8.0.2软件作图。

2 结果与分析

2.1 *ycl*突变体的表型鉴定

黄瓜叶色突变体*ycl*自幼苗出土后子叶一直呈黄化状态，无法持续自养生长发育，约2周后野生型XYYH-3-1进入真叶期，突变体枯萎死亡(图1A)，是典型的黄化致死突变体，命名为*ycl* (*yellow cotyledon lethal*)。*ycl*在播种7天时子叶打开，各农艺性状均显著低于野生型(表2)。子叶期，突变体*ycl*的株高、根长、茎粗及叶面积分别为野生型的54.32%、35.35%、81.82%和21.57%。

本研究利用XYYH-2-1-1株系进行自交，构建了18个分离群体，第3号群体XYYH-3-1的绿叶表型能稳定遗传，作为野生型；其余17个群体自交后代能分离出黄化苗，作为杂合株，其中第18号群体共22株，正常绿苗与黄化致死苗的比值为3:1，经卡方检验(χ^2=0.088 9, P>0.05)符合孟德尔遗传规律。观察*ycl*与XYYH-3-1在种子萌发过程中，黑暗处理对其生长发育及叶色的影响。黑暗培养7天后突变体*ycl*及其野

表1 qRT-PCR引物

Table 1 Primers used for qRT-PCR

Primer name	Forward primer (5′→3′)	Reverse primer (5'→3')
Cs-Actin	GTTACGCCCTCCCTCATGCCATTC	TCCCGTTCGGCAGTGGTGGT
CsaV3_3G002180	GTCGTCCTGCCATTCGATCA	AGCACCAAGTTCACTCCAACT
CsaV3_5G025230	AATTCTTCCGACCCGAACCC	AGTAGCCTTCTGCGGACCTA
CsaV3_1G030370	CAGTGGCTGGATACGTCCTC	GTGAGCTCCCGCCATAAAGT
CsaV3_7G000620	TGGAGCATCTCCGAAAGTGG	GGCAAGGAATTGTGATGCCA
CsaV3_5G028880	TAGAACCCAGGCTCCCTCAA	CCGTGTTTTCACAAGCTTCTCT
CsaV3_3G041340	AACATGTTACTGGTGGGGGC	CACATTGAAATCATTGGGTACCTG
CsaV3_6G037230	CCCACTCAAGCGATGTG CTA	CCATTGACCTCAGCATTGCG
CsaV3_5G006200	GACCCAGTTCAAGCTAGCCA	ACTGAGACAACAAGCGCGTA
CsaV3_7G008610	GGCTCCAAGGGCCAATACAT	GTAGGCCTTGGACAGGCATT

图1 *ycl*与XYYH-3-1黄瓜子叶期表型变化比较

(A) 4、5、6、7、8和14天野生型(WT)和*ycl*表型变化(自然光); **(B)** 第7天苗龄时2组WT和*ycl*表型差异(黑暗处理7天); **(C)** 第8天苗龄时2组WT和*ycl*表型差异(光照培养1天)。Bars=1 cm

Figure 1 Comparison of phenotypic changes between *ycl* and XYYH-3-1 at the cotyledon stage of cucumber

(A) Phenotypic changes of wild type (WT) and *ycl* in 4, 5, 6, 7, 8 and 14 days (natural light); **(B)** Phenotypic differences of WT and *ycl* between the two groups at 7 d of age (dark treatment for 7 d); **(C)** Phenotypic differences of WT and *ycl* between the two groups at 8 d of age (light culture for 1 d). Bars=1 cm

表2 *ycl*与XYYH-3-1黄瓜子叶期(7天)的农艺性状

Table 2 Agronomic characters of *ycl* and XYYH-3-1 at cotyledon stage (7 d) of cucumber

Material	Plant height (cm)	Root length (cm)	Stem diameter (cm)	Leaf area (cm^2)
WT	4.86±0.32	15.56±0.94	0.22±0.03	9.04±1.66
ycl	2.64±0.56**	5.5±0.9**	0.18±0.02*	1.95±0.26**

WT: 野生型。*表示差异显著(*t*检验, *P*<0.05); **表示差异极显著(*t*检验, *P*<0.01)。

WT: Wild type. * denotes significant differences (*t*-test, *P*< 0.05); ** denote extremely significant differences (*t*-test, *P*<0.01).

生型XYYH-3-1子叶皆呈黄色, *ycl*表现出不同程度的发育缺陷, 下胚轴长度显著低于野生型, 根系长度较野生型短(图1B)。光照培养1天后叶片逐渐展开, 野生型子叶转绿, *ycl*叶色无变化(图1C), 由此推测*ycl*的生长抑制表型为非光依赖型。

2.2 叶绿素及其合成中间代谢产物含量测定

与野生型(XYYH-3-1)相比, 突变体*ycl*的Chl *a*、Chl *b*、Caro和Total Chl含量均显著降低, 分别下降至野生型的0.12%、0.19%、0.14%和20.32%, 并且叶绿素*a*和叶绿素*b*的含量均趋于零。*ycl*叶绿素*a*/*b*为1.93, XYYH-3-1叶绿素*a*/*b*为3.01, 说明相较于叶绿素*b*, 突变体的叶绿素*a*含量下降幅度更大; 此外, 突变体与野生型的总叶绿素/类胡萝卜素(Total Chl/Caro)值分别为0.04和6.63 (图2B; 表3), 表明*ycl*叶片黄化的形成主要是叶绿素含量显著降低, 尤其是叶绿素*a*含量减少所致。

为了进一步探讨突变体中光合色素缺失的原因, 对叶绿素生物合成中间代谢产物含量进行测定。将野生型叶绿素合成的各种前体物质含量统一设定为100%, 结果表明, 与野生型相比, 突变体子叶中5-氨基乙酰丙酸(5-ALA)、胆色素原(PBG)、尿卟啉原III以及粪卟啉原III的含量均上升, 分别为野生型的107.56%、118.99%、158.35%和127.31%; 而原卟啉IX及Mg-原卟啉IX的含量有所降低, 为野生型的86.25%和55.31%, 但Proto IX的含量与野生型相比无显著差异(图2A)。由此推测*ycl*突变体叶绿素合成过程中Proto IX镁离子螯合受阻, 导致Mg-Proto IX积累

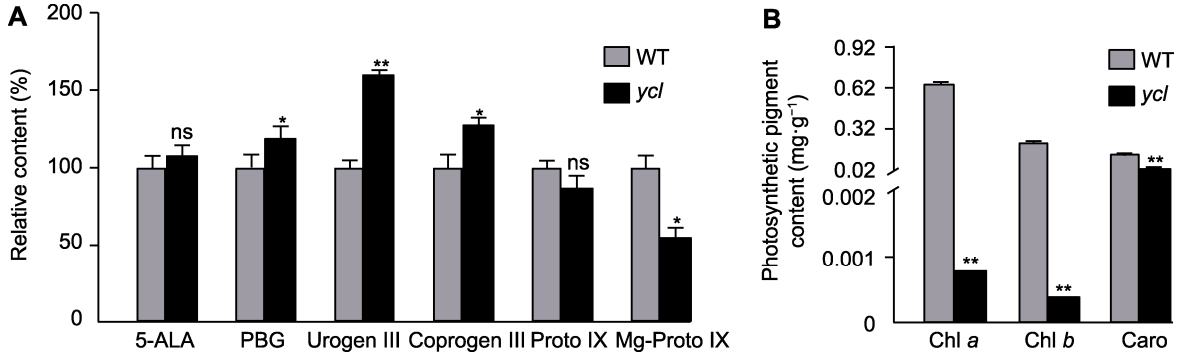

图2 *ycl*与XYYH-3-1叶绿素及其合成中间代谢产物的含量

(A) 叶绿素合成中间代谢产物的相对含量; **(B)**光合色素含量。WT: 野生型; 5-ALA: 5-氨基乙酰丙酸; PBG: 胆色素原; Urogen III: 尿卟啉原III; Coprogen III: 粪卟啉原III; Proto IX: 原卟啉IX; Mg-Proto IX: Mg-原卟啉IX。*表示差异显著(*t*检验, $P<0.05$); **表示差异极显著(*t*检验, $P<0.01$); ns表示差异不显著。

Figure 2 Content of chlorophyll and its biosynthetic intermediate metabolites in *ycl* and XYYH-3-1

(A) Relative content of chlorophyll biosynthetic intermediate metabolites; **(B)** Photosynthetic pigment content. WT: Wild type; 5-ALA: 5-aminolevulinic acid; PBG: Porphobilinogen; Urogen III: Uroporphyrinogen III; Coprogen III: Coproporphyrinogen III; Proto IX: Protoporphyrin IX; Mg-Proto IX: Mg-protoporphyrin IX. * denote significant differences (*t*-test, $P<0.05$); ** denote extremely significant differences (*t*-test, $P<0.01$); ns denote no significant difference.

表3 *ycl*和XYYH-3-1叶片的光合色素含量

Table 3 Photosynthetic pigment content in leaves of *ycl* and XYYH-3-1

Material	Chl *a* ($mg·g^{-1}$)	Chl *b* ($mg·g^{-1}$)	Caro ($mg·g^{-1}$)	Total Chl ($mg·g^{-1}$)	Chl *a*/*b*	Total Chl/Caro
WT	0.6483±0.0162	0.2157±0.0063	0.1304±0.0018	0.8641±0.0225	3.0057	6.6272
ycl	0.0008±0**	0.0004±0**	0.0265±0.0007**	0.0012±0**	1.9303	0.0443

WT: 野生型。**表示差异极显著(*t*检验, $P<0.01$)。WT: Wild type. ** denote extremely significant differences (*t*-test, $P<0.01$).

减少，使得合成通路无法合成后续产物，最终使叶绿素*a*和叶绿素*b*含量急剧降低。

2.3 *ycl*叶片叶绿体发育不良，光合能力下降

分别对*ycl*和XYYH-3-1子叶期叶片进行显微观察，发现野生型叶片中，海绵组织与栅栏组织结构饱满、排列有序且紧密(图3A, B)；突变体*ycl*中，栅栏组织和海绵组织细胞排列散乱，缺乏明确的界限，细胞之间的空隙较大，叶脉也相对较小(图3C, D)，表明*ycl*的叶片组织发育异常。用透射电镜(transmission electron microscope, TEM)观察*ycl*突变体和野生型子叶的超微结构，发现野生型叶片的叶绿体形状大多为长椭圆形或梭形，细胞内数目多(图3E)；*ycl*突变体叶片的叶绿体膨胀成近圆形(图3G)。与野生型相比，*ycl*突变体的叶绿体结构简单且发育不良，基粒片层稀疏，叶绿体内积累了大量的嗜锇体(图5H)，表明黄化致死突变体*ycl*的叶绿体发育存在明显缺陷。

*ycl*突变体和野生型子叶期叶片的光合参数测定结果显示(表4)，*ycl*的净光合速率(P_n)极显著低于野生型，说明*ycl*消耗的有机物量大于光合作用产生的有机物量。*ycl*的气孔导度(G_s)以及蒸腾速率(T_r)极显著低于野生型，分别为XYYH-3-1的37.84%和47.24%，同时伴随着胞间CO_2浓度(C_i)显著上升，CO_2消耗减少。由此推测*ycl*光合速率降低主要是气孔导度和二氧化碳利用率降低、叶绿素含量减少以及叶绿体发育异常等因素综合作用的结果。

2.4 活性氧的产生与积累

植物叶色突变通常伴随过量活性氧(reactive oxygen species, ROS)的积累，引发膜脂过氧化。在*ycl*突变体中，超氧化物歧化酶(SOD)和过氧化物酶(POD)活性均显著高于野生型(图4A, B)，表明其通过上调抗氧化酶活性清除ROS，这一适应性响应可能是缓解叶绿素缺失的补偿机制，以维持基本的生理功能。

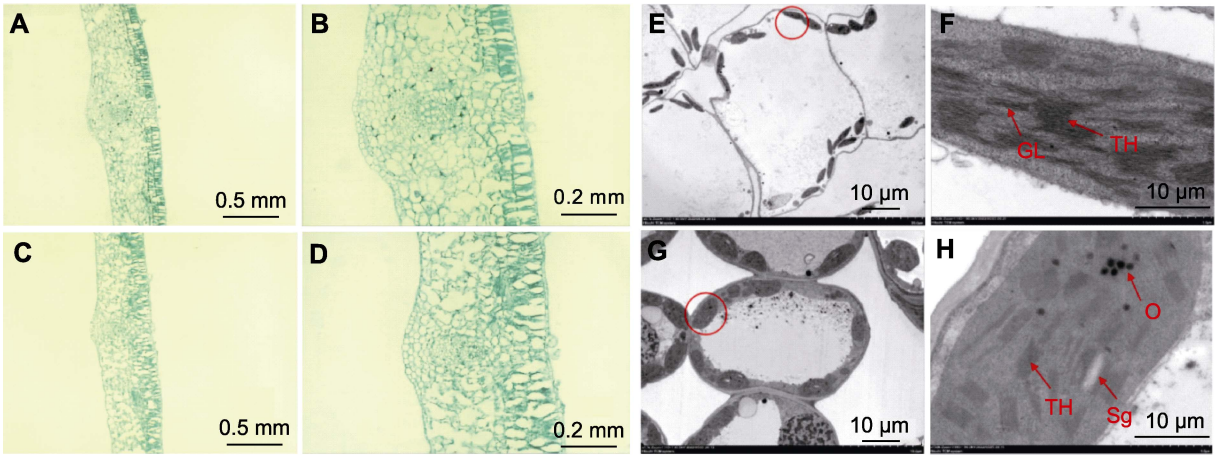

图3 *ycl*和XYYH-3-1叶片的显微结构及叶绿体超微结构

(A), (B) 野生型子叶显微结构; **(C), (D)** 突变体子叶显微结构; **(E), (F)** 野生型叶绿体超微结构; **(G), (H)** *ycl*叶绿体超微结构。**(F)**是**(E)**中红色圆圈中的叶绿体放大版。**(H)**是**(G)**中红色圆圈中的叶绿体放大版。Sg: 淀粉粒; TH: 类囊体; GL: 基粒片层; O: 嗜锇体

Figure 3 Microstructure and chloroplast ultrastructure of *ycl* and XYYH-3-1 leaves

(A), (B) Wild type cotyledon microstructures; **(C), (D)** Mutant cotyledon microstructures; **(E), (F)** Wild type chloroplast ultrastructures; **(G), (H)** *ycl* chloroplast ultrastructures. **(F)** is an enlarged version of the chloroplast in the red circle in **(E)**. **(H)** is an enlarged version of the chloroplast in the red circle in **(G)**. Sg: Starch grain; TH: Thylakoid; GL: Grana lamella; O: Osmiophilic body

表4 *ycl*和XYYH-3-1植株的光合作用参数

Table 4 Photosynthesis parameters of the *ycl* and XYYH-3-1

Material	P_n (μmol·m^{-2}·s^{-1})	G_s (mmol·m^{-2}·s^{-1})	C_i (μmol·mol^{-1})	T_r (mol·m^{-2}·s^{-1})
WT	15.85±1.39	0.37±0.08	331±12	4.53±0.62
ycl	–2.49±0.15**	0.14±0.02**	458±7**	2.17±0.31**

P_n: 净光合速率; G_s: 气孔导度; C_i: 胞间CO_2浓度; T_r: 蒸腾速率; WT: 野生型。**表示差异极显著(*t*检验, *P*<0.01)。

P_n: Net photosynthetic rate; G_s: Stomatal conductance; C_i: Intercellular CO_2 concentration; T_r: Transpiration rate; WT: Wild type. ** denote extremely significant differences (*t*-test, *P*<0.01).

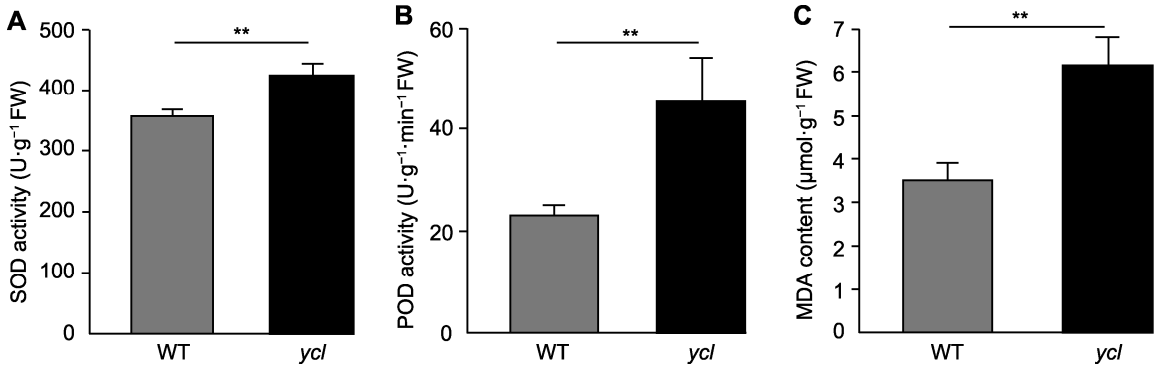

图4 *ycl*和XYYH-3-1植株的抗氧化物酶活性及丙二醛含量

(A) 超氧化物歧化酶(SOD)活性; **(B)** 过氧化物酶(POD)活性; **(C)** 丙二醛(MDA)含量。WT: 野生型. **表示差异极显著(*t*检验, *P*<0.01)。

Figure 4 Antioxidant enzyme activities and malondialdehyde contents of *ycl* and XYYH-3-1

(A) Superoxide dismutase (SOD) activity; **(B)** Peroxidase (POD) activity; **(C)** Malondialdehyde (MDA) contents. WT: Wild type. ** denote extremely significant differences (*t*-test, *P*<0.01).

ROS的大量积累会导致质膜过氧化产生丙二醛(MDA), 故MDA含量可以反映细胞膜脂质过氧化程度。*ycl*突变体中MDA含量极显著高于野生型(图4C), MDA大量积累表明突变体的细胞膜结构损伤严重。

2.5 *ycl*突变位点的初定位及候选基因筛选

为确定突变基因及其突变类型, 采用全基因组重测序结合BSA技术对分离群体进行分析, 发现第18号株系正常绿苗与黄化致死苗的比值为3:1, 经卡方检验(χ^2=0.088 9, P>0.05)符合孟德尔遗传规律; XYYH-2-1-1自交构建的18个总群体的分离单株中正常绿苗与黄化致死苗的比值为6:1。故对第18号株系进行单基因BSA分析, 取子叶构建2个DNA池; 对所有群体中的单株进行QTL分析, 取子叶构建3个DNA池; 取真叶构建3个基因池, 进一步展开全基因组重测序工作。测序数据产出和质量统计显示, 各样本Q30 (错误率在0.1%以下)均在90%以上, 对Reads中的碱基质量进行评估, GC含量占比正常, 各组测序深度均覆盖全基因组的98%以上, 样本测序质量、最终数据产量和质量均满足分析要求。

BSA混池测序结果显示, 在第18号群体中获得15 323个差异SNP, 在XY子叶群体中获得18 953个差异SNP, 在XY真叶群体中获得20 973个差异SNP, 在3个群体中获得野生亲本纯合、隐性池差异且纯合、显性池纯合或杂合的位点分别有19、51和730个SNP, 以1 000 000 bp为窗口, 100 000 bp为步长, 根据隐性池减去显性池的SNP index作图(图5), 发现3号染色体上SNP密集, 且在3个群体中有重叠。由于与目标性状关联的SNP在染色体上连锁遗传, 故将目的基因初定位在第3号染色体的1.48–1.9 Mb区间, 此候选区段中包含41个蛋白编码基因(表5), 后续将进一步精细定位以获得候选突变位点。

取*ycl*及野生型子叶期(7天)植株根、茎和叶, 利用荧光定量PCR对候选区间内*CsaV3_3G001980*基因进行表达量分析, 发现在根和茎中, *ycl*基因的表达量极显著低于野生型; 在叶中, 其表达量极显著高于野生型(图5)。*CsaV3_3G001980*编码NPF (NITRATE TRANSPORTER 1/PEPTIDE TRANSPORTER FAMILY)蛋白, 与拟南芥NRT1.5编码基因同源, NRT1.5参与硝酸盐从根到茎的木质部运输, 推测*ycl*突变体中该基因的表达量下降会影响硝酸盐的运输, 导致叶色发生变化。候选基因*CsaV3_3G001980*序列全长为6 364 bp, 设计包含启动子区在内的*CsaV3_3G001980* gDNA引物, 分段进行克隆测序, 对测序数据拼接并比对, 结果证实未发生基因突变。

2.6 *ycl*与XYYH-3-1转录组比较分析

2.6.1 转录组数据的评估与检验

*ycl*及其野生型植株播种40小时后取样进行转录组测序, 数据显示每组样品的Clean reads均高于6.1×10^9, 参考基因组比对率mapped Reads均高于96%。原始数据过滤后测序数据的碱基准确率Q20 (错误率在1%以下)均在96%以上, Q30 (错误率在0.1%以下)均在91%以上, GC含量均介于44%–45%之间。与黄瓜参考基因组进行比对, 发现6组样品的Clean reads与蛋白质编码序列区域的比对率均超过88%, 证明转录组测序数据质量完好。

为验证RNA-Seq数据的可靠性, 从差异表达基因(differentially expressed genes, DEGs)中随机选取8个基因进行qRT-PCR分析, 包括UMC编码基因(*CsaV3_1G030370*)、F-box编码基因(*CsaV3_3G041340*)、AtCKX6编码基因(*CsaV3_5G006200*)、Chlase1编码基因(*CsaV3_5G025230*)、PEPC4编码基因(*CsaV3_5G028880*)、TwTPS28编码基因(*CsaV3_6G037230*)、生长素诱导蛋白X10A编码基因(*CsaV3_7G000620*)和细胞色素P450 707A4编码基因(*CsaV3_7G008610*)。结果显示, 这8个基因的转录组数据与qRT-PCR相对表达量一致, 证实了转录组数据的可信度(图6D)。

2.6.2 基因GO富集和KEGG通路富集分析

以|$\log_2$ (Fold Change)|>1并且q-value<0.05为标准, 进一步筛选野生型和*ycl*突变体的差异表达基因。在*ycl*与野生型植株中共鉴定到337个DEGs, 148个DEGs上调, 189个DEGs下调(图6A)。对差异表达基因进行GO富集和KEGG富集分析, 在各GO条目中(图6C), 与生物过程相关的DEGs主要集中于细胞过程(cellular process)、代谢过程(metabolic process)和刺激反应(response to stimulus)三大功能类别。与分子功能相关的DEGs主要集中于四吡咯结合(tetrapyrrole binding)、血红素结合(heme binding)和铁离子结合(iron ion binding)等, 以上过程大部分与光合色素合成相关, 表

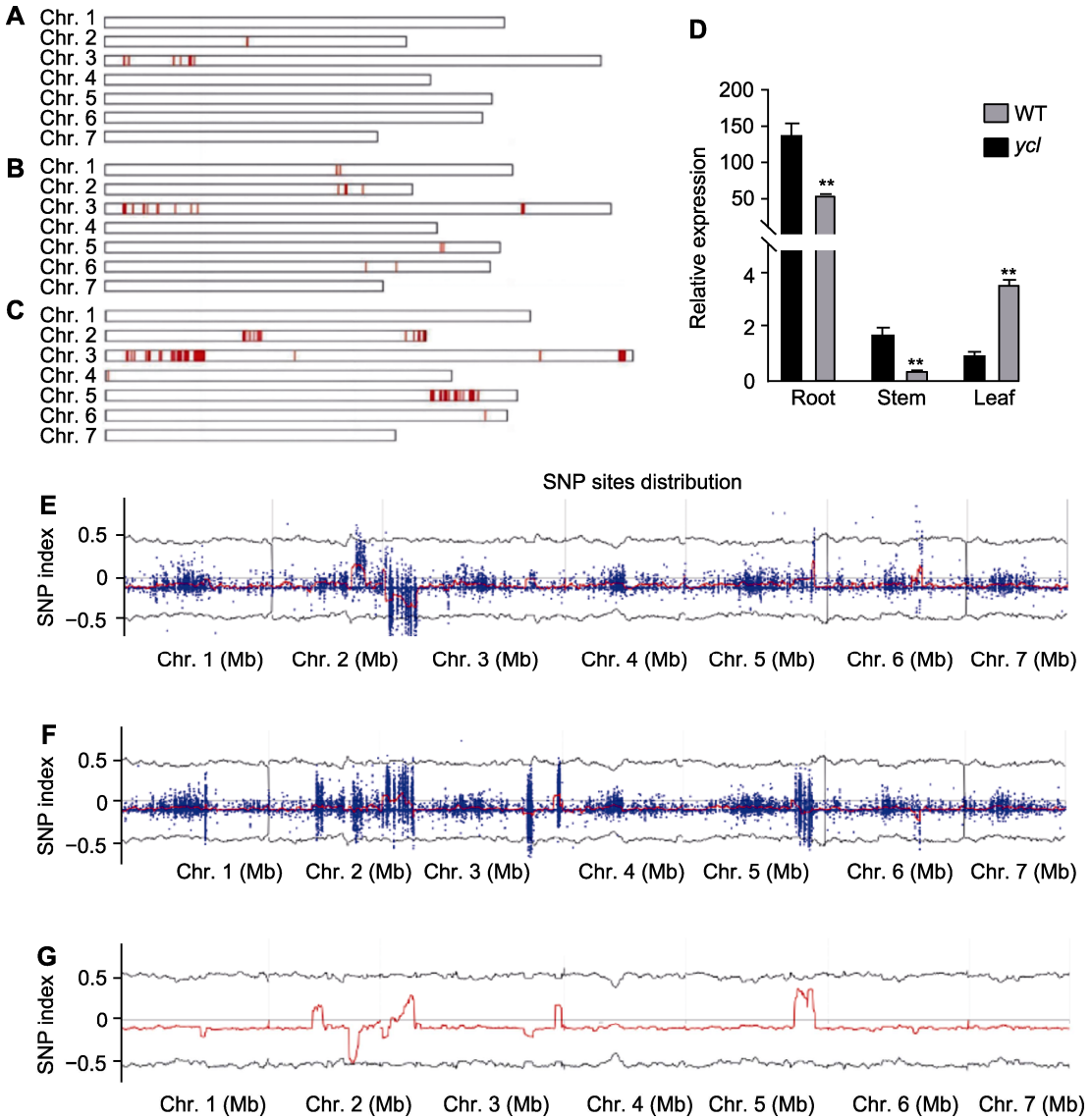

图5 突变基因的初定位及筛选

(A)–(C) 单核苷酸多态性分布(**(A)** 第18号群体; **(B)** XY子叶群体; **(C)** XY真叶群体); **(D)** *CsaV3_3G001980*相对表达量(**表示差异极显著, *t*检验, $P<0.01$); **(E)–(G)** SNP index峰图(**(E)** 第18号群体; **(F)** XY子叶群体; **(G)** XY真叶群体)。WT: 野生型; SNP: 单核苷酸多态性

Figure 5 Preliminary localisation and screening of mutant genes

(A)–(C) Distribution of single nucleotide polymorphisms (**(A)** Population 18; **(B)** XY cotyledon population; **(C)** XY true leaf population); **(D)** Relative expression of *CsaV3_3G001980* (** denote extremely significant differences, *t*-test, $P<0.01$); **(E)–(G)** SNP index plot (**(E)** Population 18; **(F)** XY cotyledon population; **(G)** XY true leaf population). WT: Wild type; SNP: Single nucleotide polymorphism

明*ycl*叶色突变涉及色素合成与光合作用; 同时, 部分DEGs聚集在氧化还原酶活性(oxidoreductase activity)和过氧化物酶活性(peroxidase activity)上, 说明突变体氧化还原平衡受损。与细胞组分相关的DEGs主要富集于液泡(vacuole)、细胞壁(cell wall)、凯氏带(casparian strip)、质体类囊体膜基质侧(stromal side of plastid thylakoid membrane)、线粒体(mitochondrion)和内质网小体, 说明突变体的细胞发育受到影响。

表5 *ycl*突变位点初定位区间内基因

Figure 5 The genes within the preliminarily mapped region of *ycl* mutant site

Genes within the interval	Annotation
CsaV3_3G001960	Cytochrome P450 family ent-kaurenoic acid oxidase
CsaV3_3G001970	Cytochrome P450 family ent-kaurenoic acid oxidase
CsaV3_3G001980	Protein NRT1/PTR FAMILY 7.3-like
CsaV3_3G001990	Hsp90 co-chaperone Cdc37, N-terminally processed like
CsaV3_3G002000	Ribose-phosphate pyrophosphokinase
CsaV3_3G002010	Type I inositol polyphosphate 5-phosphatase, puta
CsaV3_3G002020	Phenylalanine-tRNA ligase alpha subunit like
CsaV3_3G002030	Two-component response regulator-like aprr2
CsaV3_3G002040	S-adenosyl-L-methionine-dependent methyltransferases superfamily protein
CsaV3_3G002050	Vacuolar protein sorting-associated protein 55 homolog
CsaV3_3G002060	Haloacid dehalogenase-like hydrolase
CsaV3_3G002070	Haloacid dehalogenase-like hydrolase domain-containing protein
CsaV3_3G002080	Regulator of nonsense transcripts 1 homolog
CsaV3_3G002090	Lon protease homolog 2, peroxisomal
CsaV3_3G002100	Electron carrier/iron ion-binding protein
CsaV3_3G002110	BOI-related E3 ubiquitin-protein ligase 1
CsaV3_3G002120	Protein of unknown function (DUF581)
CsaV3_3G002130	Poly(U)-specific endoribonuclease
CsaV3_3G002140	Methyltransferase-like protein 13
CsaV3_3G002150	Beta-amylase
CsaV3_3G002160	Protein kinase, putative
CsaV3_3G002170	Novel plant snare, putative
CsaV3_3G002180	Phosphatidylinositol 4-phosphate 5-kinase 1
CsaV3_3G002190	Coiled-coil domain-containing protein 97
CsaV3_3G002200	Calcineurin B-like protein
CsaV3_3G002210	Unknown protein
CsaV3_3G002220	Protein kinase
CsaV3_3G002230	Unknown protein
CsaV3_3G002240	Bifunctional inhibitor/plant lipid transfer protein/seed storage helical domain-containing protein
CsaV3_3G002250	Peptidyl-prolyl *cis-trans* isomerase-like
CsaV3_3G002260	DVA-1 polyprotein
CsaV3_3G002270	tRNA/rRNA methyltransferase (SpoU) family protein
CsaV3_3G002280	Protein lingerer like
CsaV3_3G002290	Chlorophyll *a*/*b* binding family protein
CsaV3_3G002300	ATP-dependent Clp protease proteolytic subunit
CsaV3_3G002310	Unknown protein
CsaV3_3G002320	Histone-lysine N-methyltransferase, H3 lysine-9 specific SUVH6-like
CsaV3_3G002330	Kelch repeat-containing protein
CsaV3_3G002340	GATA transcription factor 26-like
CsaV3_3G002350	Vesicle-associated protein 2-1
CsaV3_3G002360	50S ribosomal protein L19, chloroplastic

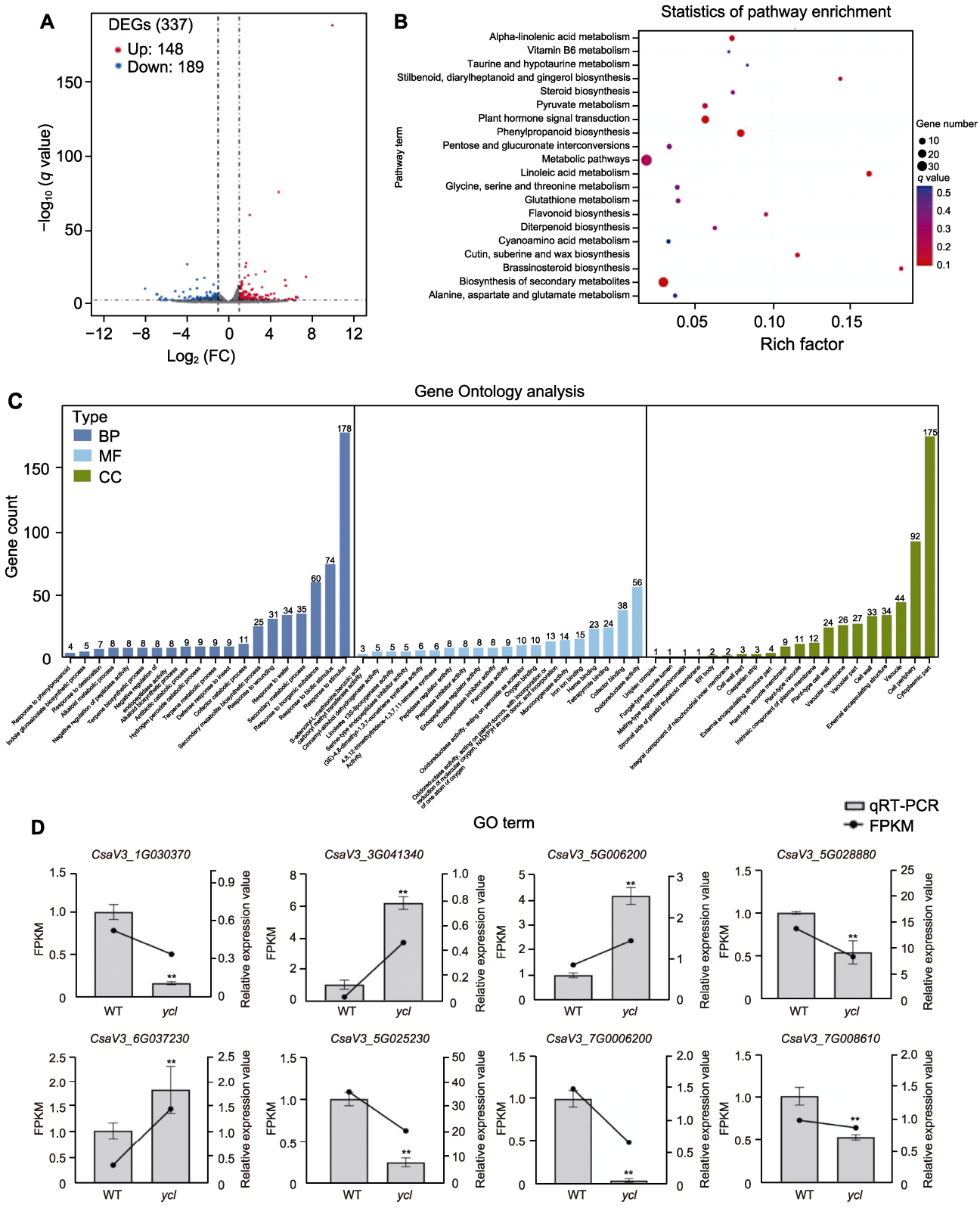

图6 *ycl*与XYYH-3-1间的RNA-Seq分析

(A) 差异表达基因火山图; **(B)** 差异表达基因KEGG途径富集散点图; **(C)** GO term二级分类统计结果; **(D)** 转录组结果的qRT-PCR验证。BP: 生物过程; MF: 分子功能; CC: 细胞组分; WT: 野生型; DEG: 差异表达基因; FPKM: 每千碱基转录本每百万映射片段数; FC: 倍性变化。**表示差异极显著(*t*检验, $P<0.01$)。

Figure 6 RNA-Seq analysis of differential expression between *ycl* and XYYH-3-1
(A) Differentially expressed genes volcano map; **(B)** Scatter plot of differentially expressed genes KEGG pathway enrichment; **(C)** GO term secondary classification statistics; **(D)** The qRT-PCR verification of transcriptome results. BP: Biological process; MF: Molecular function; CC: Cellular component; WT: Wild type; DEG: Differential expressed gene; FPKM: Fragments per kilobase per million mapped reads; FC: Fold Change. ** denote extremely significant differences (*t*-test, $P<0.01$).

为深入探究差异表达基因所涉及的生化代谢以及相关信号转导途径，对差异表达基因进行KEGG Pathway聚类分析(图6B)。结果显示，差异表达基因最显著富集的通路有4条，分别为代谢途径(metabolic pathways) (富集于此的基因有39个)、次生代谢物生物合成(biosynthesis of secondary metabolites) (富集于此的基因有30个)、植物激素信号转导(plant hormone signal transduction) (富集于此的基因有15个)和苯丙素的生物合成(phenylpropanoid biosynthesis) (富集于此的基因有14个)。

2.6.3 黄瓜黄化致死突变体表型相关DEGs的筛选与分析

为进一步揭示黄化致死表型形成的原因，对高度相关的差异表达基因进行筛选分析。在转录组差异表达基因中，发现5个参与光合作用的关键基因(图7A)，分别为1个编码叶绿素*a*/*b*结合蛋白(chlorophyll *a*/*b* binding protein, LHCP)的基因、2个编码质体蓝素(plastocyanin, PC)的基因、1个编码磷酸烯醇式丙酮酸羧化酶(phosphoenolpyruvate carboxylase, PEPC)且富集于光合生物中的碳固定基因和1个编码叶绿素酶1 (Chlase 1)的基因。与野生型相比，前4个基因在突变体*ycl*中表达下调，后1个基因表达上调。

类黄酮被划分为六大类，其在植物体内以黄酮、查尔酮、花青素和前花青素等多种形式存在，类黄酮物质不仅影响植株的呈色，还是植物抗逆过程中的重要物质。本研究中，通过转录组测序发现类黄酮生物合成通路上存在2个DEGs（图7B)，其中编码黄酮3′,5′-甲基转移酶(如咖啡酰辅酶A-3-O甲基转移酶(*trans*-caffeoyl-CoA 3-O-methyltransferase, CCoA-MT))的基因上调，编码Vinorine合成酶(如司替木丹碱-O-乙酰转移酶(stemmadenine O-acetyltransferase, SAT))的基因显著下调，说明突变体*ycl*中黄酮类物质的合成代谢受到调控，影响了叶片呈色。前人研究发现，花青素完成聚合需要先与转运蛋白结合。多药和有毒物排出家族(multidrug and toxic compound extrusion, MATE)转运蛋白和谷胱甘肽*S*-转移酶(glutathione-*S*-transferase, GST)被证实参与花青素的转运过程，GST还在植物生长发育和非生物胁迫响应中发挥多种作用。我们在转录组差异表达基因中发现5个参与此过程的关键基因，2个基因编码GST，3个基因编码MATE转运蛋白(图7C)，编码ABC转运蛋白的基因表达下调也表明突变体中活性氧高度积累，说明*ycl*的花青素跨膜或囊泡转运及抗氧化功能受到一定影响。转录因子也可能是导致突变体产生叶色突变的重要指标之一，转录组测序分析发现*ycl*及其野生型之间存在7个编码转录因子的差异表达基因(图7D)，5个编码bHLH转录因子，且全部下调表达，2个编码MYB转录因子，说明突变体的花青素含量发生变化，极有可能影响了叶片呈色。

3 讨论

黄瓜作为研究葫芦科的模式植物，仅被报道了6种致死型叶色突变体。与之前的叶色突变体表型不同，本研究鉴定的黄瓜叶色突变体*ycl*是通过人工筛选在自然突变条件下获得的典型黄化致死突变体，生长抑制表型为非光依赖型，说明其突变涉及的生理生化途径与形态建成初期的生长抑制相关；同时，*ycl*黄化致死表型受单基因隐性遗传控制。综上，黄瓜黄化致死突变体*ycl*是一种新型的叶色突变体，可作为叶绿素代谢和叶绿体发育等相关机制研究的理想材料。

植物叶色变化在很大程度上是色素含量变化的外在表现(Chen et al., 2013; Liu et al., 2021)；同时还伴随不同程度的叶绿体结构缺失(Lin et al., 2022; Cheng et al., 2022; Amaresh et al., 2023)。Sandhu等(2016)研究发现，大豆黄化突变体*yl*总叶绿素含量相比野生型减少62.88%，但可繁殖后代；而突变体*yv*类囊体膜更薄，光合色素减少92.66%，属于致死型黄化突变。本研究中，*ycl*突变株的光合色素含量变化趋势与突变体*9110 Gt*相同(Miao et al., 2016)，Chl *a*和Chl *b*含量趋于零，Chl *a*含量下降幅度大于Chl *b*，

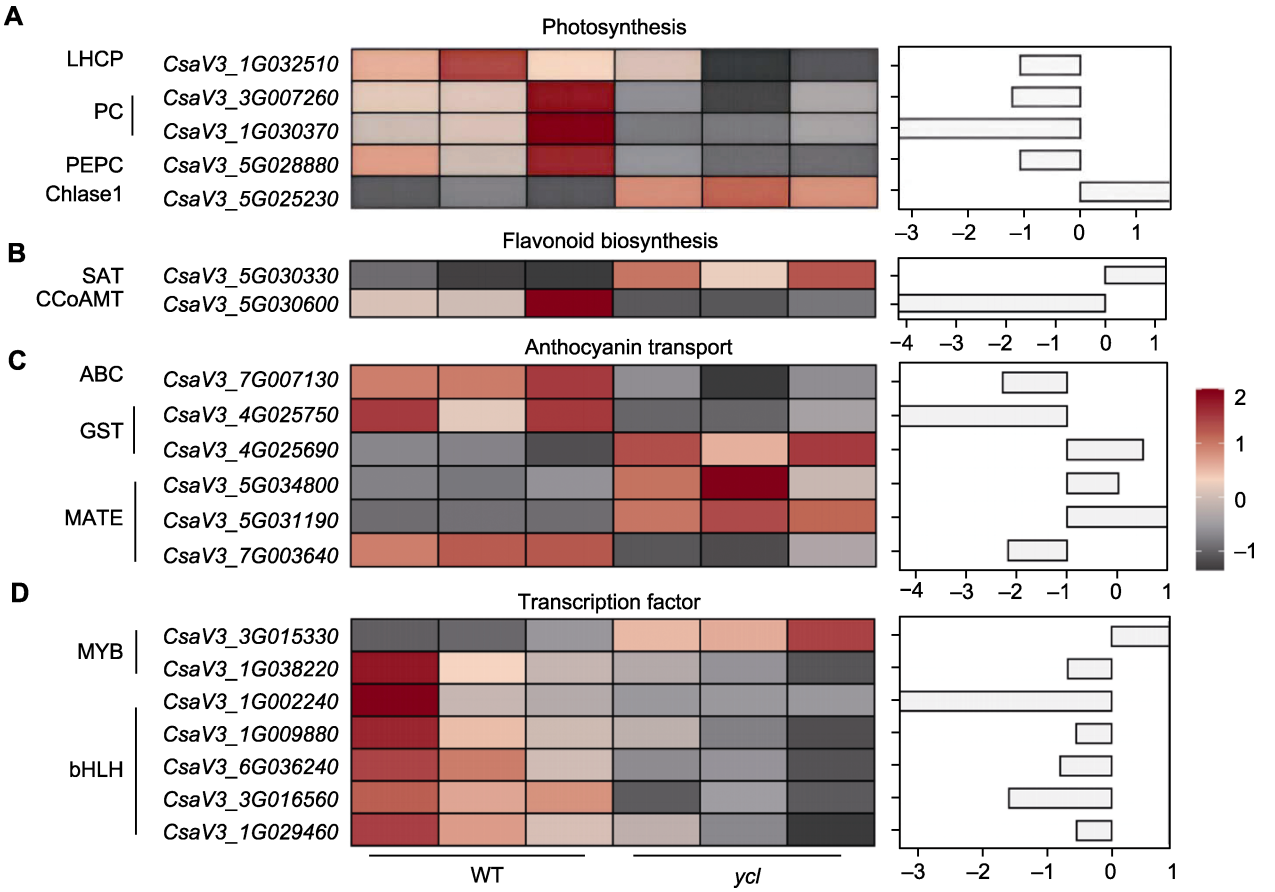

图7 与*ycl*表型相关的差异表达基因(DEGs)

(A) 涉及光合作用的DEGs; **(B)** 涉及类黄酮生物合成的DEGs; **(C)** 涉及花青素转运的DEGs; **(D)** 编码转录因子的DEGs。WT: 野生型; LHCP: 叶绿素*a*/*b*结合蛋白; PC: 质体蓝素; PEPC: 磷酸烯醇式丙酮酸羧化酶; Chlase1: 叶绿素酶1; SAT: 司替木丹碱-O-乙酰转移酶; CCoAMT: 咖啡酰辅酶A-3-O甲基转移酶; GST: 谷胱甘肽*S*-转移酶; MATE: 多药和有毒物排出家族

Figure 7 Differentially expressed genes (DEGs) associated with the *ycl* phenotype

(A) DEGs involved in photosynthesis; **(B)** DEGs involved in flavonoid biosynthesis; **(C)** DEGs involved in anthocyanin transport; **(D)** DEGs encoding transcription factors. WT: Wild type; LHCP: Chlorophyll *a*/*b* binding protein; PC: Plastocyanin; PEPC: Phosphoenolpyruvate carboxylase; Chlase1: Chlorophyllase 1; SAT: Stemmadenine O-acetyltransferase; CCoAMT: *Trans*-caffeoyl-CoA 3-O-methyltransferase; GST: Glutathione-*S*-transferase; MATE: Multidrug and toxic compound extrusion

类胡萝卜素含量也极显著降低, 这与前人报道的类胡萝卜素含量相对增加的突变体*ygl1*相反(Ding et al., 2019)。Zhang等(2006)通过对叶绿素合成前体物质相对含量进行测定, 发现水稻突变体*hl1*以及*chl9*的Mg-Proto IX含量分别下降至野生型的25%和31%, 这与*ycl*的测定结果类似, 推测*ycl*突变体叶绿素含量大幅降低源于Proto IX中镁离子的螯合过程受阻。同时, 超微结构显示*ycl*中叶绿体膨胀成近圆形, 这一表型与大豆黄化突变体*yl* (Sandhu et al., 2016)叶绿体的体积增大类似。大豆*yl*叶绿体异常源于叶绿体核糖体功能缺陷导致的蛋白质合成障碍, 这与*ycl*中编码叶绿体50S核糖体蛋白L19的候选基因*CsaV3_3G002360*功能相似, 其功能缺失可能通过干扰核糖体的组装, 引发类似的翻译系统崩溃, 最终导致叶绿体结构异常和黄化致死表型。光合色素的含量以及分布也决定了叶片的光合能力(Tanaka and Tanaka, 2011; Deng et al., 2017)。与野生型相比, *ycl*中P_n极显著降低, C_i浓度上升, 这与大豆黄化突变体*VS-5Y* (李超汉等, 2019)一致。综上所述, 突变体*ycl*光合作用受损可能由气孔导度降低、叶绿素含量减少和叶绿体发育受阻等多重因素所致。

转录组测序(RNA-Seq)分析结果中, 部分DEGs

富集在氧化还原酶活性、氧化还原过程和类囊体膜基质侧，说明突变株体内ROS含量过高，而ROS作为信号分子调控叶绿素合成基因表达，导致叶绿体类囊体膜结构的稳定性及叶绿素含量显著降低。这与通过透射电镜观察到的叶绿体结构发育异常一致，也与*ycl*子叶期SOD和POD活性及MDA含量显著高于野生型相符。Du等(2020)发现岷江百合(*Lilium regale*)突变体*lrysl1*中调控光合途径的*CP43*和*PetE*等基因下调会导致光合系统受损，最终呈现黄化致死表型。本研究中突变体*ycl*亦有参与光合途径的DEGs，如编码叶绿素*a*/*b*结合蛋白的基因*LHCP*和富集在光合作用天线蛋白上的基因*PC*。*ycl*中*LHCP*和*PC*等基因显著下调表达，直接削弱了光能捕获与电子传递能力，导致光合效率极低以及最终上游的叶绿素合成异常；而叶绿素酶1表达上调，加速了下游的叶绿素降解，二者共同造成叶绿素积累受阻，导致叶绿素含量趋近于零。同时，极低的光合效率导致ATP供应不足，削弱了SOD和POD的抗氧化能力，ROS进一步破坏叶绿体结构，加剧了代谢紊乱，这一机制暗示*ycl*可能代表一种新型的非光依赖型致死调控模块。

花青素、叶绿素和类胡萝卜素在叶片中所占的比例及分布直接影响植物叶片的呈色(Jiao et al., 2020; Gao et al., 2021)。我们在*ycl*中发现5个DEGs参与花青素的转运，包括维持植物细胞活性氧平衡的ABC转运蛋白(Awai et al., 2006; Zhu et al., 2019)、通过转运原花青素前体参与花青素合成的MATE转运蛋白(Sun et al., 2022)，及参与植物生长发育、次生代谢、逆境抗性和花青素跨膜运输的GST转运蛋白(Jiang et al., 2019; Ghangal et al., 2020)。本文的研究结果表明，*ycl*的叶色变化与花青素的转运合成途径受调控相关。同时，RNA-Seq分析结果显示，*ycl*中有2个编码转录因子MYB的差异表达基因，5个编码bHLH转录因子的差异表达基因且均下调。MYB在植物次生代谢、逆境应答以及形态建成中发挥重要作用(Qiu et al., 2014; Boase et al., 2015; Zhou et al., 2015)。bHLH作为MBW (MYB-bHLH-WD40)复合物中的转录因子，通过与MYB协同互作激活结构基因以促进原花青素的合成(Allan et al., 2008; Butelli et al., 2008; Zhou et al., 2015; Xie et al., 2016; Dasgupta et al., 2017)。因此，编码转录因子的DEGs可能导致突变体的花青素含量发生变化；同时，下游光合作用和抗氧化基因无法激活，使代谢紊乱，最终导致叶色改变。由此可见，突变体*ycl*黄化致死表型是多基因层级调控失效的结果，包括叶绿素代谢失衡、ROS积累与氧化胁迫及转录因子网络失调等。

4 结论

本研究通过全基因组重测序结合BSA-Seq定位*ycl*突变基因，将*ycl*黄化致死突变基因初定位于第3号染色体的1.48–1.9 Mb区域。在已克隆的8个黄瓜叶色基因中，仅有黄色幼叶突变体*C777* (Hu et al., 2020)和绿叶突变体*104Y* (Zhang et al., 2020b)的突变基因定位于3号染色体。*C777*具有黄色子叶和带绿点的真叶，后期叶片转绿。*104Y*的子叶和前五叶期的真叶呈黄色。结合基因注释以及转录组分析候选基因，对参与硝酸盐木质部运输(Lin et al., 2008)的基因*CsaV3_3G001980*进行qRT-PCR分析及测序验证，发现该基因的表达量在*ycl*的根和茎中极显著低于野生型，但在叶中显著高于野生型，通过测序扩增发现*ycl*中该基因无突变。基于此，今后在考虑表观调控的同时，需对候选区域开发更多的分子标记，进一步扩大作图群体，缩小突变基因所在的范围。

作者贡献声明

赵蔓雅和孙倩楠：完成实验、分析数据和撰写论文初稿；徐晶晶、段恬妮和蔡锦涛：协助完成实验；周婧和范婷婷：指导论文修改；萧浪涛和王若仲：构思并设计实验、修改论文。

参考文献

Allan AC, Hellens RP, Laing WA (2008). MYB transcription factors that colour our fruit. *Trends Plant Sci* **13**, 99–102.

Amaresh, Krishnan SG, Vinod KK, Chinnusamy V, Sevanthi ACRMV, Dhandapani R, Ellur RK, Bhowmick PK, Bollinedi H, Umadevi P, Senapati M, Verma RK, Nagarajan M, Dhawan G, Kumar P, Singh AK (2023). Phenotypic characterization of the novel seedling stage zebra leaf mutant, Pusa Zebra 18 in rice. *Plant Physiol Rep* **28**, 500–512.

Awai K, Xu CC, Tamot B, Benning C (2006). A phosphatidic acid-binding protein of the chloroplast inner envelope membrane involved in lipid trafficking. *Proc Natl Acad Sci USA* **103**, 10817–10822.

Boase MR, Brendolise C, Wang L, Ngo H, Espley RV, Hellens RP, Schwinn KE, Davies KM, Albert NW (2015). Failure to launch: the self-regulating *Md-MYB10$_{R6}$* gene from apple is active in flowers but not leaves of *Petunia*. *Plant Cell Rep* **34**, 1817–1823.

Bogorad L (1962). Porphyrin synthesis. *Methods Enzymol* **5**, 885–895.

Butelli E, Titta L, Giorgio M, Mock HP, Matros A, Peterek S, Schijlen EGWM, Hall RD, Bovy AG, Luo J, Martin C (2008). Enrichment of tomato fruit with health-promoting anthocyanins by expression of select transcription factors. *Nat Biotechnol* **26**, 1301–1308.

Chen H, Cheng ZJ, Ma XD, Wu H, Liu YL, Zhou KN, Chen YL, Ma WW, Bi JC, Zhang X, Guo XP, Wang JL, Lei CL, Wu FQ, Lin QB, Liu YQ, Liu LL, Jiang L (2013). A knockdown mutation of *YELLOW-GREEN LEAF2* blocks chlorophyll biosynthesis in rice. *Plant Cell Rep* **32**, 1855–1867.

Chen JY, Zhao J, Liu X, Li C, Lin DZ, Dong YJ, Ye SH, Zhang XM (2010). Genetic analysis and molecular mapping of a new thermosensitive leaf-color mutant in *Oryza sativa*. *Chin Bull Bot* **45**, 419–425. (in Chinese)
陈佳颖, 赵剑, 刘晓, 李超, 林冬枝, 董彦君, 叶胜海, 张小明 (2010). 一个新水稻温敏感叶色突变体的遗传分析及其基因分子定位. 植物学报 **45**, 419–425.

Cheng MZ, Meng FY, Mo FL, Chen XL, Zhang H, Wang AX (2022). Insights into the molecular basis of a yellow leaf color mutant (*ym*) in tomato (*Solanum lycopersicum*). *Sci Hortic* **293**, 110743.

Dasgupta K, Thilmony R, Stover E, Oliveira ML, Thomson J (2017). Novel R2R3-MYB transcription factors from *Prunus americana* regulate differential patterns of anthocyanin accumulation in tobacco and citrus. *GM Crops Food* **8**, 85–105.

Dei M (1985). Benzyladenine-induced stimulation of 5-aminolevulinic acid accumulation under various light intensities in levulinic acid-treated cotyledons of etiolated cucumber. *Physiol Plant* **64**, 153–160.

Deng LC, Qin P, Liu Z, Wang GL, Chen WL, Tong JH, Xiao LT, Tu B, Sun YT, Yan W, He H, Tan J, Chen XW, Wang YP, Li SG, Ma BT (2017). Characterization and fine-mapping of a novel premature leaf senescence mutant *yellow leaf and dwarf 1* in rice. *Plant Physiol Biochem* **111**, 50–58.

Ding Y, Yang W, Su CG, Ma HH, Pan Y, Zhang XG, Li JH (2019). Tandem 13-lipoxygenase genes in a cluster confers yellow-green leaf in cucumber. *Int J Mol Sci* **20**, 3102.

Du WK, Hu FR, Yuan SX, Liu C (2020). The identification of key candidate genes mediating yellow seedling lethality in a *Lilium regale* mutant. *Mol Biol Rep* **47**, 2487–2499.

Gao ML, Hu LL, Li YH, Weng YQ (2016). The chlorophyll-deficient *golden leaf* mutation in cucumber is due to a single nucleotide substitution in *CsChlI* for magnesium chelatase I subunit. *Theor Appl Genet* **129**, 1961–1973.

Gao YF, Zhao DH, Zhang JQ, Chen JS, Li JL, Weng Z, Rong LP (2021). *De novo* transcriptome sequencing and anthocyanin metabolite analysis reveals leaf color of *Acer pseudosieboldianum* in autumn. *BMC Genomics* **22**, 383.

Ghangal R, Rajkumar MS, Garg R, Jain M (2020). Genome-wide analysis of glutathione *S*-transferase gene family in chickpea suggests its role during seed development and abiotic stress. *Mol Biol Rep* **47**, 2749–2761.

Guan HY, Xu XB, He CM, Liu CX, Liu Q, Dong R, Liu TS, Wang LM (2016). Fine mapping and candidate gene analysis of the leaf-color gene *ygl-1* in maize. *PLoS One* **11**, e0153962.

Han HW, Zhou Y, Liu HF, Chen XJ, Wang Q, Zhuang HM, Sun XX, Ling QH, Zhang HJ, Wang BK, Wang J, Tang YP, Wang H, Liu HY (2023). Transcriptomics and metabolomics analysis provides insight into leaf color and photosynthesis variation of the yellow-green leaf mutant of hami melon (*Cucumis melo* L.). *Plants* **12**, 1623.

Hu LL, Zhang HQ, Xie C, Wang J, Zhang JY, Wang H, Weng YQ, Chen P, Li YH (2020). A mutation in *CsHD* encoding a histidine and aspartic acid domain-containing protein leads to *yellow young leaf-1* (*yyl-1*) in cucumber (*Cucumis sativus* L.). *Plant Sci* **293**, 110407.

Huang SN, Liu ZY, Li DY, Yao RP, Hou L, Li X, Feng H (2016). Physiological characterization and comparative transcriptome analysis of a slow-growing reduced-thylakoid mutant of Chinese cabbage (*Brassica campestris* ssp. *pekinensis)*. *Front Plant Sci* **7**, 3.

Huang WF, Zhang Y, Shen LQ, Fang Q, Liu Q, Gong CB, Zhang C, Zhou Y, Mao C, Zhu YL, Zhang JH, Chen HP, Zhang Y, Lin YJ, Bock R, Zhou F (2020). Accumulation of the RNA polymerase subunit RpoB depends on RNA editing by OsPPR16 and affects chloroplast development during early leaf development in rice. *New Phytol* **228**, 1401–1416.

Jiang SH, Chen M, He NB, Chen XL, Wang N, Sun QG, Zhang TL, Xu HF, Fang HC, Wang YC, Zhang ZY, Wu SJ, Chen XS (2019). MdGSTF6, activated by MdMYB1, plays an essential role in anthocyanin accumulation in apple. *Hortic Res* **6**, 40.

Jiao FC, Zhao L, Wu XF, Song ZB, Li YP (2020). Metabolome and transcriptome analyses of the molecular mechanisms of flower color mutation in tobacco. *BMC Genomics* **21**, 611.

Ladygin VG (2006). Spectral features and structure of chloroplasts under an early block of chlorophyll synthesis. *Biophysics* **51**, 635–644.

Li CH, Zhu LH, Yang HJ, Song RH, Gu WH (2019). Main agronomic characters and biochemical traits of xantha mutant of vegetable soybean. *Mol Plant Breed* **17**, 3726–3734. (in Chinese)
李超汉，朱丽华，杨红娟，宋荣浩，顾卫红 (2019). 菜用大豆黄化新突变体的主要农艺性状和生理特性. 分子植物育种 **17**, 3726–3734.

Li XF, Zhang ZL (2016). Plant Physiology Laboratory Manual (5th edn). Beijing: Science Press. pp. 30–31. (in Chinese)
李小方，张志良 (2016). 植物生理学实验指导(第5版). 北京: 科学出版社. pp. 30–31.

Lin N, Gao YM, Zhou QY, Ping XK, Li JN, Liu LZ, Yin JM (2022). Genetic mapping and physiological analysis of chlorophyll-deficient mutant in *Brassica napus* L. *BMC Plant Biol* **22**, 244.

Lin SH, Kuo HF, Canivenc G, Lin CS, Lepetit M, Hsu PK, Tillard P, Lin HL, Wang YY, Tsai CB, Gojon A, Tsay YF (2008). Mutation of the *Arabidopsis NRT1.5* nitrate transporter causes defective root-to-shoot nitrate transport. *Plant Cell* **20**, 2514–2528.

Liu J, Wang JY, Yao XY, Zhang Y, Li JQ, Wang XX, Xu ZJ, Chen WF (2015). Characterization and fine mapping of thermo-sensitive chlorophyll deficit mutant1 in rice (*Oryza sativa* L.). *Breed Sci* **65**, 161–169.

Liu L, Sun TT, Liu XY, Guo Y, Huang X, Gao P, Wang XZ (2019). Genetic analysis and mapping of a striped rind gene (*st3*) in melon (*Cucumis melo* L.). *Euphytica* **215**, 20.

Liu P, Li MJ (2016). Experiments in Plant Physiology (2nd edn). Beijing: Science Press. pp. 142–150. (in Chinese)
刘萍，李明军 (2016). 植物生理学实验(第2版). 北京: 科学出版社. pp. 142–150.

Liu X, Huang QQ, Yang YR, Tang JY, Zhao YN, Zhang J (2021). Characterization and map-based cloning of the novel rice yellow leaf mutant *yl3*. *J Plant Biol* **64**, 35–44.

Mao GZ, Wei HL, Hu W, Ma Q, Zhang M, Wang HT, Yu SX (2019). Fine mapping and molecular characterization of the virescent gene *vsp* in upland cotton (*Gossypium hirsutum*). *Theor Appl Genet* **132**, 2069–2086.

Miao H, Zhang SP, Wang M, Wang Y, Weng YQ, Gu XF (2016). Fine mapping of virescent leaf gene *v-1* in cucumber (*Cucumis sativus* L.). *Int J Mol Sci* **17**, 1602.

Michelmore RW, Paran I, Kesseli RV (1991). Identification of markers linked to disease-resistance genes by bulked segregant analysis: a rapid method to detect markers in specific genomic regions by using segregating populations. *Proc Natl Acad Sci USA* **88**, 9828–9832.

Nagata N, Tanaka R, Satoh S, Tanaka A (2005). Identification of a vinyl reductase gene for chlorophyll synthesis in *Arabidopsis thaliana* and implications for the evolution of prochlorococcus species. *Plant Cell* **17**, 233–240.

Parks BM, Quail PH (1991). Phytochrome-deficient *hy1* and *hy2* long hypocotyl mutants of *Arabidopsis* are defective in phytochrome chromophore biosynthesis. *Plant Cell* **3**, 1177–1186.

Pierce LK, Wehner TC (1990). Review of genes and linkage groups in cucumber. *Hortscience* **25**, 605–615.

Qin R, Zeng DD, Liang R, Yang CC, Akhter D, Alamin M, Jin XL, Shi CH (2017). Rice gene *SDL/RNRS1*, encoding the small subunit of ribonucleotide reductase, is required for chlorophyll synthesis and plant growth development. *Gene* **627**, 351–362.

Qiu J, Sun SQ, Luo SQ, Zhang JC, Xiao XZ, Zhang LQ, Wang F, Liu SZ (2014). *Arabidopsis* AtPAP1 transcription factor induces anthocyanin production in transgenic *Taraxacum brevicorniculatum*. *Plant Cell Rep* **33**, 669–680.

Sakowska K, Alberti G, Genesio L, Peressotti A, Delle Vedove G, Gianelle D, Colombo R, Rodeghiero M, Panigada C, Juszczak R, Celesti M, Rossini M, Haworth M, Campbell BW, Mevy JP, Vescovo L, Cendrero-Mateo MP, Rascher U, Miglietta F (2018). Leaf and canopy photosynthesis of a chlorophyll deficient soybean mutant. *Plant Cell Environ* **41**, 1427–1437.

Sandhu D, Atkinson T, Noll A, Johnson C, Espinosa K, Boelter J, Abel S, Dhatt BK, Barta T, Singsaas E, Sepsenwol S, Goggi AS, Palmer RG (2016). Soybean proteins GmTic110 and GmPsbP are crucial for chloroplast development and function. *Plant Sci* **252**, 76–87.

Schmittgen TD, Livak KJ (2008). Analyzing real-time PCR data by the comparative C(T) method. *Nat Protoc* **3**, 1101–1108.

Shim KC, Kang YN, Song JH, Kim YJ, Kim JK, Kim C, Tai TH, Park I, Ahn SN (2023). A frameshift mutation in the Mg-chelatase I subunit gene *OsCHLI* is associated with a lethal chlorophyll-deficient, yellow seedling phenotype in rice. *Plants* **12**, 2831.

Song MF, Wei QZ, Wang J, Fu WY, Qin XD, Lu XM, Cheng F, Yang K, Zhang L, Yu XQ, Li J, Chen JF, Lou QF (2018). Fine mapping of *CsVYL*, conferring virescent leaf through the regulation of chloroplast development in cucumber. *Front Plant Sci* **9**, 432.

Stern DB, Hanson MR, Barkan A (2004). Genetics and genomics of chloroplast biogenesis: maize as a model system. *Trends Plant Sci* **9**, 293–301.

Sun Y, Bai PP, Gu KJ, Yang SZ, Lin HY, Shi CG, Zhao YP (2022). Dynamic transcriptome and network-based analysis of yellow leaf mutant *Ginkgo biloba*. *BMC Plant Biol* **22**, 465.

Tanaka R, Tanaka A (2011). Chlorophyll cycle regulates the construction and destruction of the light-harvesting complexes. *Biochim Biophys Acta Bioenerg* **1807**, 968–976.

Wu ZM, Zhang X, He B, Diao LP, Sheng SL, Wang JL, Guo XP, Su N, Wang LF, Jiang L, Wang CM, Zhai HQ, Wan JM (2007). A chlorophyll-deficient rice mutant with impaired chlorophyllide esterification in chlorophyll biosynthesis. *Plant Physiol* **145**, 29–40.

Xie Y, Tan HJ, Ma ZX, Huang JR (2016). DELLA proteins promote anthocyanin biosynthesis via sequestering MYBL2 and JAZ suppressors of the MYB/bHLH/WD40 complex in *Arabidopsis thaliana*. *Mol Plant* **9**, 711–721.

Xiong LR, Du H, Zhang KY, Lv D, He HL, Pan JS, Cai R, Wang G (2021). A mutation in *CsYL2.1* encoding a plastid isoform of triose phosphate isomerase leads to *yellow leaf 2.1* (*yl2.1*) in cucumber (*Cucumis sativus* L.). *Int J Mol Sci* **22**, 322.

Xu BH, Zhang CY, Gu Y, Cheng R, Huang DY, Liu X, Sun YD (2023). Physiological and transcriptomic analysis of a yellow leaf mutant in watermelon. *Sci Rep* **13**, 9647.

Yin JJ, Zhu XB, Yuan C, Wang J, Li WT, Wang YP, He M, Cheng QS, Ye BQ, Chen WL, Linghu QY, Wang JC, Ma BT, Qin P, Li SG, Chen XW (2015). Characterization and fine mapping of a novel vegetative senescence lethal mutant locus in rice. *J Genet Genomics* **42**, 511–514.

Zhang HT, Li JJ, Yoo JH, Yoo SC, Cho SH, Koh HJ, Seo HS, Paek NC (2006). Rice *Chlorina-1* and *Chlorina-9* encode ChlD and ChlI subunits of Mg-chelatase, a key enzyme for chlorophyll synthesis and chloroplast development. *Plant Mol Biol* **62**, 325–337.

Zhang KJ, Li Y, Zhu WW, Wei YF, Njogu MK, Lou QF, Li J, Chen JF (2020b). Fine mapping and transcriptome analysis of virescent leaf gene *v-2* in cucumber (*Cucumis sativus* L.). *Front Plant Sci* **11**, 570817.

Zhang TT, Dong XY, Yuan X, Hong YY, Zhang LL, Zhang X, Chen SX (2022). Identification and characterization of *CsSRP43*, a major gene controlling leaf yellowing in cucumber. *Hortic Res* **9**, uhac212.

Zhao CJ, Liu LJ, Safdar LB, Xie ML, Cheng XH, Liu YY, Xiang Y, Tong CB, Tu JX, Huang JY, Liu SY (2020a). Characterization and fine mapping of a yellow-virescent gene regulating chlorophyll biosynthesis and early stage chloroplast development in *Brassica napus*. *G3* (Bethesda) **10**, 3201–3211.

Zhong XM, Sun SF, Li FH, Wang J, Shi ZS (2015). Photosynthesis of a yellow-green mutant line in maize. *Photosynthetica* **53**, 499–505.

Zhou H, Lin-Wang K, Wang HL, Gu C, Dare AP, Espley RV, He HP, Allan AC, Han YP (2015). Molecular genetics of blood-fleshed peach reveals activation of anthocyanin biosynthesis by NAC transcription factors. *Plant J* **82**, 105–121.

Zhu HY, Zhang MJ, Sun SR, Yang S, Li JX, Li H, Yang HH, Zhang KG, Hu JB, Liu DM, Yang LM (2019). A single nucleotide deletion in an ABC transporter gene leads to a dwarf phenotype in watermelon. *Front Plant Sci* **10**, 1399.

Zhu XY, Guo S, Wang ZW, Du Q, Xing YD, Zhang TQ, Shen WQ, Sang XC, Ling YH, He GH (2016). Map-based cloning and functional analysis of *YGL8*, which controls leaf colour in rice (*Oryza sativa*). *BMC Plant Biol* **16**, 134.

Identification, Mapping and Transcriptome Analysis of a New Leaf Color Mutant in Cucumber

Manya Zhao, Qiannan Sun, Jingjing Xu, Tianni Duan, Jintao Cai, Jing Zhou, Tingting Fan
Langtao Xiao*, Ruozhong Wang*

Hunan Provincial Key Laboratory of Phytohormones and Growth Development, College of Bioscience and Biotechnology Hunan Agricultural University, Changsha 410128, China

INTRODUCTION: Cucumber (*Cucumis sativus*) is one of the foremost vegetable crops globally. Photosynthesis intricately influences the fruit yield of cucumber, and leaf color determines the photosynthetic efficiency to a large extent. Therefore, Leaf color mutants serve as ideal materials for scrutinizing diverse physiological processes, including photomorphogenesis, chloroplast development, chlorophyll metabolism, and photosynthetic mechanisms. Currently, the molecular mechanisms underlying the yellowing lethal phenotype remain unclear.

RATIONALE: In this study, a stable cucumber yellowing lethal mutant, *ycl* (*yellow cotyledon lethal*), was isolated from the near-isogenic line XYYH-2-1-1. The phenotype, leaf microstructure and chloroplast ultrastructure, as well as physiological

and biochemical analyses, were conducted on the mutant *ycl* and the wild-type XYYH-3-1 to explore the physiological mechanisms underlying the yellowing lethal phenotype. Preliminary localisation of yellowing lethal mutation genes was performed by whole genome resequencing using BSA. The integration of transcriptome sequencing allowed us to analyze the expression of genes related to yellowing death and the main pathways. This approach laid a solid foundation for further investigation into the molecular mechanisms responsible for the lethal phenotype associated with *ycl* yellowing.

RESULTS: The *ycl* mutant exhibited yellow cotyledons, which ultimately withered and perished within approximately two weeks. Notably, its growth-inhibiting phenotype appeared to be light-independent. Compared to the wild type, *ycl* accumulated extremely low Chl *a* and Chl *b* contents, which was consistent with the blockade in the magnesium ion chelation process within the chlorophyll biosynthesis pathway. Microscopic and ultrastructural analyses revealed disordered *ycl* leaf structure and inhibited chloroplast development. Additionally, the *ycl* mutant displayed significantly increased antioxidant enzyme activities and malondialdehyde contents, suggesting elevated oxidative stress levels and robust antioxidant capacities. The substantial decrease in net photosynthetic rate and rise in intercellular CO_2 concentration in *ycl* were hypothesized to stem from reduced stomatal conductance, diminished chlorophyll content, and impaired chloroplast development in the mutant. Transcriptomic analyses suggested that key pathways including photosynthesis, flavonoid biosynthesis, chlorophyll metabolism, and reactive oxygen species metabolism were affected in *ycl*. The *ycl* mutant gene was preliminarily mapped to a region between 1.48 to 1.9 Mb on chromosome 3 through BSA-seq analysis, encompassing 41 candidate genes.

CONCLUSION: The study investigated the physiological mechanisms underlying the yellowing lethal phenotype of the *ycl* mutant, preliminarily mapped the mutant gene to chromosome 3, and identified differentially expressed genes (DEGs) and key pathways associated with the lethal phenotype. These findings provide valuable insights into the molecular mechanisms of chloroplast development in cucumber.

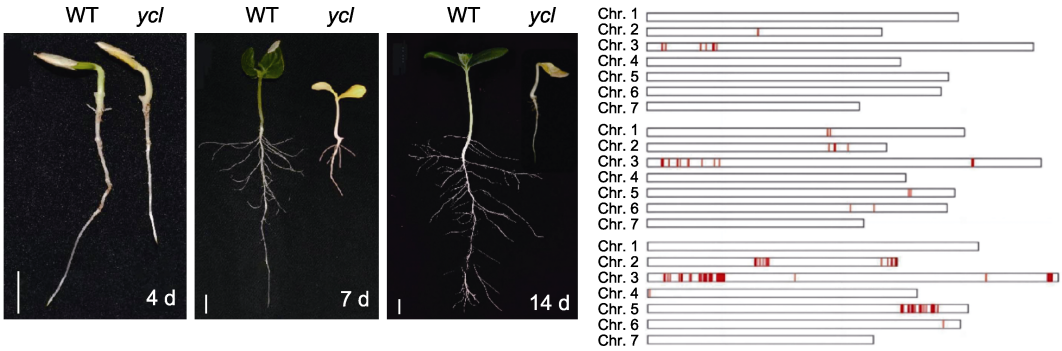

Phenotypic changes of WT and the *ycl* mutant at the cotyledon stage under natural light conditions, and preliminary mapping of the mutant gene.

Key words cucumber, yellowing lethal mutant *ycl*, physiological characteristics, gene mapping, transcriptome analysis

Zhao MY, Sun QN, Xu JJ, Duan TN, Cai JT, Zhou J, Fan TT, Xiao LT, Wang RZ (2025). Identification, mapping and transcriptome analysis of a new leaf color mutant in cucumber. *Chin Bull Bot* **60**, 515–532.

* Authors for correspondence. E-mail: ltxiao@hunau.edu.cn; wangruozhong@hunau.edu.cn

(责任编辑: 孙冬花)